Article ID: 1000-7032(2024)05-0699-12

Tetradentate Pt(Ⅱ) Complex Sensitized Multi-resonant Thermally Activated Delayed Fluorescence for Narrow Bandwidth Blue Solution-processed OLEDs

LI Jiale[1], FANG Hui[1], GONG Shaolong[1*], XIE Guohua[1,2*]

(1. *Sauvage Center for Molecular Sciences, Hubei Key Lab on Organic and Polymeric Optoelectronic Materials, Department of Chemistry, Wuhan University, Wuhan* 430072, *China*;
2. *The Institute of Flexible Electronics (Future Technologies), Xiamen University, Xiamen* 361005, *China*)

**Corresponding Authors, E-mail: slgong@whu. edu. cn; ifeghxie@xmu. edu. cn*

Abstract: Although organic light-emitting diodes (OLEDs) have been commercialized and become popular in smartphone, the vacuum deposition process makes them too expensive for mass production and less cost-effective. Herein, we employed highly emissive platinum complex as the sensitizer and multi-resonant thermally activated delayed fluorescence (MR-TADF) molecules as the emitters to demonstrate highly efficient, high color purity, and solution-processed OLEDs with the alleviated efficiency roll-offs. The triplet excitons are rapidly converted to singlet excitons assisted by the phosphorescent sensitizer. Attributed to the reduced triplet exciton lifetime induced by the phosphorescent sensitizer, the MR-TADF OLEDs exhibited a maximum external quantum efficiency (EQE) of 13.2% with a low efficiency roll-off of 25.8% at 1 000 cd/m^2. To reduce Dexter energy transfer between phosphorescence sensitizer and the emitter, an analogue TADF emitter with the peripheral bulky blocking units was employed, which rendered an improved maximum EQE of 13.6%. This investigation presents a general approach to realize high-performance solution-processed electroluminescence.

Key words: phosphorescent sensitizer; narrow bandwidth, multi-resonance; thermally activated delayed fluorescence; organic light-emitting diodes

CLC number: O482.31; TN312.8 **Document code**: A **DOI**: 10.37188/CJL.20240049

基于四配位铂配合物敏化多重共振热激活延迟荧光的窄发射蓝色溶液加工有机发光二极管

李家乐[1], 方 辉[1], 龚少龙[1*], 谢国华[1,2*]

(1. 武汉大学 化学与分子科学学院, 索维奇分子科学中心, 湖北 武汉 430072;
2. 厦门大学 柔性电子(未来技术)研究院, 福建 厦门 361005)

摘要: 有机发光二极管(OLED)已经在智能手机方面获得了商业应用,由于目前规模生产的OLED采用蒸镀工艺,使其价格居高不下。为此,我们采用溶液加工方法,使用铂配合物作为敏化剂,多重共振热激活延迟荧光材料作为发光分子,实现了高效、高色纯度、低效率滚降的器件开发。磷光敏化剂的引入可使三线态激子高效转化为单线态激子。得益于磷光敏化剂较短的激子寿命,基于溶液加工的蓝色多重共振热激活延迟荧光器

收稿日期: 2024-02-28; **修订日期**: 2024-03-07
基金项目: 国家自然科学基金(52373195, 62175189); 江汉大学光电化学材料与器件教育部重点实验室开放基金项目(JDGD-202301); 国家自然科学基金委员会与瑞典科研与教育国际合作基金会合作交流项目(52211530052)
Supported by National Natural Science Foundation of China(52373195, 62175189); Opening Project of Key Laboratory of Optoelectronic Chemical Materials and Devices, Ministry of Education, Jianghan University(JDGD-202301); Joint China-Sweden Mobility Program(52211530052)

件不仅实现了13.2%的外量子效率，而且在1 000 cd/m^{2}亮度下的效率滚降仅为25.8%。为了进一步抑制Dexter能量转移，我们采用具有外围位阻但发光核相同的分子作为客体，可使外量子效率提升至13.6%，并抑制光谱展宽。该研究为设计高色纯度、高效率的溶液加工器件提供了一个通用的策略。

关 键 词：磷光敏化；窄光谱；多重共振；热激活延迟荧光；有机发光二极管

1 Introduction

In recent years, there has been an increasing research on organic light-emitting diodes (OLEDs)[1-3]. Due to the fascinating features, such as spontaneous emission, flexibility, wide color gamut, wide viewing angles, and rapid response, OLEDs have been widely recognized as the next generation of advanced display technology[4-6]. OLEDs will be widely applied in terminal products such as solid-state lighting, TV, smartphones, tablets, and so on[7-10]. For display applications, how to simultaneously achieve high efficiency, high color purity, and low efficiency roll-off is still an appealing issue that needs to be addressed urgently.

To achieve high efficiency, it is necessary to achieve high utilization ratio of excitons[11-12]. Under the electric field, an organic emitter typically generates 25% singlet excitons and 75% triplet excitons, according to the spin statistics. Fluorescent materials typically utilize only 25% of the electrically generation excitons, *i. e.*, singlets, resulting in a relatively low exciton utilization rate. In contrast, phosphorescent molecules, benefiting from the heavy atom effect, can enhance spin-orbit coupling and thus achieve 100% utilization efficiency of excitons[13]. With the molecular engineering, researchers have designed and synthesized numerous thermally activated delayed fluorescence (TADF) molecules and hot-exciton molecules[14-17]. The triplet excitons of these molecules, due to their ability to convert triplet excitons into singlet excitons, can be harvested for photon generation. With the multiple resonance (MR) effects in TADF molecules, the unity utilization of triplet excitons and bright emission with the narrow spectral bandwidth could be simultaneously achieved. In 2016, Hatakeyama *et al.* firstly proposed the molecular design strategy of MR-TADF[18]. Such molecules generally exhibit a very high photoluminescence quantum yield (PLQY) and a small full-width at half-maximum (FWHM) less than 40 nm, which is advantageous for improving color purity[19-20]. In recent years, the development of MR-TADF materials is booming[21-22], leading to the creation of highly efficient and narrowband OLEDs.

Sensitization strategies represent another effective approach to achieve highly efficient and low efficiency roll-off OLEDs[23]. The key to this approach lies in the selection of the sensitizers. After capturing excitons by sensitizers, the emitters can generate photons *via* energy transfer from sensitizers to emitters, thereby increasing the proportion of singlet excitons of TADF molecules[24-25]. Sensitizers generally exhibit PLQYs and rapid radiative transition rates. The common sensitizers for OLEDs currently include TADF molecules, hot exciton molecules, and phosphorescent molecules[26-29]. Moreover, triplet-triplet annihilation (TTA) is an effective mechanism for exciton utilization. In such process, two triplet excitons can combine with each other to form a high-energy singlet exciton[30]. According to the characteristics of such molecules, this mechanism plays a significant role in improving the efficiency roll-off under high current conditions[31]. For TADF molecules as sensitizers, excitons in the triplet states undergo a rapid reverse intersystem crossing (RISC) process, transforming into singlet excitons[32]. In a sensitized emitting layer, Förster resonance energy transfer (FRET) frequently plays a dominant role in radiative emission[33]. For instance, the theoretical upper limit of exciton utilization ratio for fluorescent molecules is only 25%, with a maximum device efficiency of ca. 5%. However, by employing sensitization approach, it is possible to surpass the efficiency limitations of fluorescent molecules and achieve 100% exciton utilization[34]. Many highly efficient hyperfluorescent devices have

been realized based on this method[35]. Introducing phosphorescent molecules as sensitizers in the emissive layer of OLEDs is another method to fully utilize excitons owing to the FRET process from the triplet state of phosphor-sensitizer to the singlet state of the emitter[36-37]. At present, OLED based on Ir(Ⅲ) and Pt(Ⅱ) complexes based sensitizers have been demonstrated[38-39].

As mentioned above, MR-TADF molecules are very attrative due to their characteristics of high efficiency and high color purity. However, the molecules often possess long exciton lifetime, which would lead to serious efficiency roll-off under high driving current[23,40]. The issue could be addressed by introducing the sensitizers with short exciton lifetime[41]. So far, the majority of high-performance MR-TADF OLEDs have been fabricated by vacuum deposition. Nevertheless, this processing technique is associated with the expensive equipment, complicated procedures, and low material utilization[42-43]. Solution processing is an alternative method for large-area OLED mass production, offering unique advantages such as operation at room temperature and atmospheric pressure, as well as material saving. It represents a more cost-effective approach for commercialization. However, it is challenge to design and demonstrate the solution-processed high-performance MR-TADF OLEDs with the simplified structures.

Herein, we proposed an effective strategy of employing the blue tetradentate platinum phosphorescent complex PtON1 as a phosphor-sensitizer for the solution-processed blue MR-TADF OLEDs with high efficiency, alleviated efficiency roll-off and narrowband emission. PtON1 features the outstanding emission characteristics with a high PLQY and a short exciton lifetime, which are highly required as a sensitizer. When using the blue MR emitter of CzBN with the expanded conjugation skeleton, the maximum external quantum efficiency (EQE) of the solution-processed OLED reached 13.2%, and the efficiency roll-off was only 25.8% at a brightness of 1 000 cd/m^2. To further enhance device efficiency and suppress Dexter energy transfer (DET) between the sensitizer and guest emitter, the tert-butyl-modified CzBN, *i.e.*, BCzBN, was utilized as the emitter. Following sensitization, the maximum EQE was further increased to 13.6%.

2 Experiment

2.1 Materials

The modified hole injection layer, *i.e.*, PEDOT:PSS-HJ-1 was purchased from Jinghang Optoelectronics (Shenzhen) Corporation. The electron injection material lithium 8-hydroxyquinolinolate(Liq) was purchased from Xi'an Polymer Light Technology Corporation. The host materials 1,3-bis(carbazol-9-yl) benzene (mCP), the electron transporting materials 1,3,5-tri(m-pyrid-3-ylphenyl) benzene (TmPyPB), and the hole blocking layer bis[2-(diphenylphosphino)phenyl] ether oxide (DPEPO) were purchased from Luminescence Technology Corporation. The phosphor-sensitizer (PtON1) and MR-TADF emitters (CzBN and BCzBN) were synthesized by our group according to literature. All the purchased materials were used as received without further purification.

2.2 Photophysical Measurement

UV-Vis absorption spectra were recorded on a Shimadzu UV-2700 spectrophotometer. Photoluminescence (PL) spectra were processed on a Hitachi F-4600 fluorescence spectrophotometer. The transient PL decay curves were obtained by FluoTime 300 (PicoQuant GmbH) with a Picosecond Pulsed UV-LASER (LASER375) as the excitation source. The absolute PLQYs were performed with a Quantaurus-QY measurement system (C9920-02, Hamamatsu Photonics), and all the samples were excited at 300 nm.

2.3 Transient PL Spectra Fitting Method

τ_p and τ_d represent the prompt and decay fluorescence lifetimes, respectively, which were determined from the transient PL decay spectra based on the following below equations:

$$I(t) = A_1 e^{(-\tau/\tau_1)} + A_2 e^{(-\tau/\tau_2)} + A_3 e^{(-\tau/\tau_3)}, \quad (1)$$

$$\tau_{av} = \frac{\sum A_i \tau_i^2}{A_i \tau_i}, \quad (2)$$

where $I(t)$ is the fitted function of the measured transient PL decay spectra, A_i is the constants for lifetime τ_i, and the average lifetime τ_{av} is calculated

from Eq. (2).

2.4 Device Fabrication and Characterization

The indium-tin oxide (ITO) coated glasses were used as the substrates. Firstly, the substrates were cleaned by ultrasonic treatment in acetone and ultrasonic ethanol, consecutively. Afterwards, the substrates were dried with N_2 and treated in a UV-ozone chamber for 20 min. The PEDOT: PSS-HJ-1 was spin-coated at 4 000 r/min on the ITO substrates and then annealed at 120 ℃ for 10 min inside the N_2-filled glovebox. The emissive layer was prepared by mixing the mCP (10 mg/mL), PtON1 (5 mg/mL) and MR-TADF (CzBN, BCzBN) (1 mg/mL) in chlorobenzene solution to meet the weight ratio of 99∶0∶1, 94∶5∶1, 79∶20∶1 and 69∶30∶1, then spin-coated at 1 000 r/min for 30 s onto the hole injecting layer PEDOT: PSS-HJ-1, and then annealed at 50 ℃ for 10 min. The other layers, including DPEPO (10 nm), TmPyPB(50 nm), Liq(1 nm), and Al (100 nm) were consecutively thermally evaporated in a high vacuum chamber. Afterwards, all the devices were tested at ambient air after encapsulation with UV-curable resin. The EL spectra and the current density-voltage-luminance (*J-V-L*) characteristics were simultaneously recorded by a PR735 fluorescence spectrophotometer and a computer-controlled source meter (Keithley 2400).

3 Results and Discussion

In order to investigate the phosphorescent sensitization strategy for enhancing exciton utilization, improving device efficiency, and alleviating efficiency roll-off, the energy transfer mechanisms of the phosphor-sensitized emitting layer are schematically depicted in Fig. 1(b). Meanwhile, the chemical structures of the host, the phosphor-sensitizer, and the emitters are shown in Fig. 1(a). Herein, PtON1 was employed as the sensitizer[44], while CzBN and BCzBN were two narrowband MR-TADF molecules[45]. For MR-TADF materials, their long triplet exciton lifetimes could be magnituded of tens or even hundreds of microseconds. This would lead to significant exciton quenching and thus result in low exciton utilization.

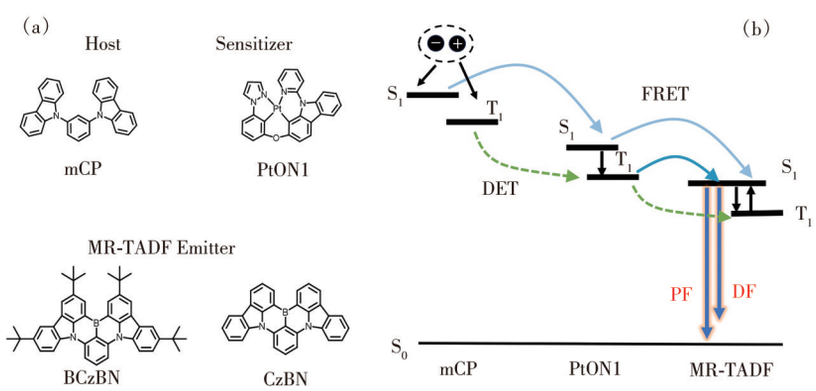

Fig.1 (a) Chemical structures of the molecules used in the emitting layers. (b) Schematic diagram of energy transfer mechanisms in the sensitized system

As shown in Fig. 1(b), the key aspect of energy transfer was FRET from PtON1 to MR-TADF molecules. In the PtON1 sensitized OLED, the T_1 energy level of mCP is 2.91 eV, which is higher than the S_1 energy level of PtON1 (2.82 eV). Meanwhile, the T_1 energy level of PtON1 (2.74 eV) is higher than the S_1 energy level of CzBN (2.59 eV) and BCzBN (2.49 eV), respectively. The singlet excitons of mCP could be transferred to the singlet excitons of PtON1 through long-range FRET processes. Since PtON1 exhibits more efficient radiative decay from the triplet state, an additional channel of FRET turns to be possible and more efficient, right from the triplet state of the sensitizer to the singlet state of MR-TADF molecule assisted by the well-matched spectral overlap shown in Fig. 2. This is because the sensitizer PtON1 displayed exciton lifetime of only a few microseconds, much shorter than the MR-TADF emitters. Therefore, Dexter energy transfer is inefficient as the terminal emitter is slightly doped. The triplet excitons in the sensitizer can

quickly transfer to the MR-TADF emitters under photoexcitation or electroexcitation. This not only enhances the exciton utilization but also suppresses efficiency loss at high brightness.

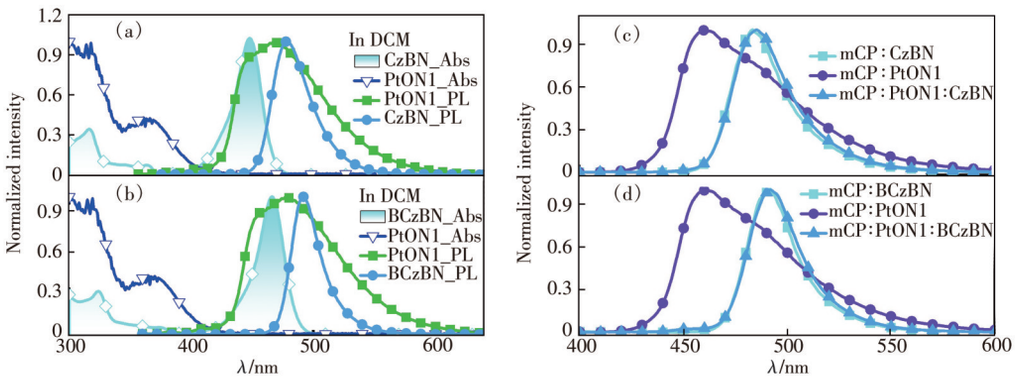

Fig.2　UV-Vis absorption spectrum and normalized PL spectra of CzBN(a) and BCzBN(b) in DCM solution(10^{-5} mol·L^{-1}, 300 K), respectively. The cases of PtON1 were provided for comparison. Normalized PL spectra of the sensitized films with CzBN(c) and BCzBN(d). The PL spectra of the binary host:guest films with PtON1 and the MR-emitters were provided as reference, respectively

To demonstrate the potential for more effective FRET between the PtON1 and the emitter, it was necessary to ensure a significant overlap between the PL spectrum of the phosphor-sensitizer and the absorption spectra of the emitters. Meanwhile, maintaining appropriate molecular distance between the sensitizer and the guest molecule was crucial to inhibit non-radiative DET processes. The intermolecular distance can be regulated by controlling the sensitizer doping concentration or introducing guest molecules with sterically hindering groups. The ultraviolet-visible (UV-Vis) absorption and photoluminescence (PL) spectroscopy of the sensitizer PtON1 and the MR-TADF molecules CzBN and BCzBN were depicted in Fig. 2(a) and 2(b). The large overlap between the PL spectrum of PtON1 and the absorption spectrum of CzBN or BCzBN indicated potentially FRET from PtON1 to the MR-TADF emitters. To prove complete FRET process, the PL spectra were further recorded from the films of mCP: 5%(wt, the same below) PtON1: 1% CzBN or BCzBN and mCP: 5% PtON1 (Fig. 2(c) and 2(d). In the doped films, the main emission peak of PtON1 was located at 461 nm with a FWHM of 57 nm, since its PL spectrum was quite broad ranging from 420 nm to 600 nm. The emission peaks of the films with mCP: CzBN and mCP: BCzBN were located at 483 nm and 490 nm, respectively. In the sensitized films, the PL spectra of the films were narrowed down to 32 nm and 29 nm, respectively. The PL spectra of the PtON1 sensitized CzBN and BCzBN films were almost identical to that of the MR emitters, respectively. This indicated that the complete energy transfer had occurred between PtON1 and CzBN, as well as PtON1 and BCzBN. The detailed photophysical data for PtON1, CzBN and BCzBN were compared in Tab. 1.

Tab. 1　The photophysical properties of the phosphorescent sensitizer and MR-TADF emitters

Materials	PL_{max}/nm[a]	S_1/T_1/eV[b]	HOMO/LUMO/eV[c]	PLQY/%[d]	τ_p/τ_d/(ns/μs)[e]	k_{RISC}/(10^4 s^{-1})[f]
CzBN	483	2.59/2.47	−5.62/−2.91	99	6.7/52.8	1.69
BCzBN	490	2.49/2.38	−5.55/−2.90	95	5.8/98.3	1.48
PtON1	461	2.82/2.74	−5.29/−2.26	82	N.A./2.2	N.A.

[a] Photoluminescence peak wavelength measured in the doped film with a host of mCP. [b] These values were obtained from the literature[44-45]. [c] HOMO: highest occupied molecular orbital and LUMO: lowest unoccupied molecular orbital. These values were obtained from the literature[44-45]. [d] Measured in the doped mCP film. [e] Prompt and delayed fluorescence(or phosphorescence for PtON1) lifetime measured in the doped mCP films. [f] Reverse intersystem crossing rate constant. N.A.: not available.

Furthermore, as shown in Fig. 3(a) and 3(b), the PL spectra and PLQY of mCP:x% PtON1:1% CzBN or BCzBN films (x = 0, 5, 20, 30) were tested (also shown in Tab. S1). Even with a high doping concentration up to 30%, the PL emission primarily originated from the radiative processes of CzBN and BCzBN, respectively, further confirming complete energy transfer between PtON1 and the guest molecules. Nevertheless, the higher PtON1 concentration led to a slight red-shift in emission and a slight spectral broadening. In the mCP:PtON1:CzBN films, the emission peaks red-shifted from 483 nm to 489 nm, accompanied with the slight enlarged FWHM to 35 nm. In contrast, in the mCP:PtON1:BCzBN films, the PL peak wavelength shifted from 490 nm to 494 nm. As the PtON1 weight ratio increased from 0% to 30%, the PL intensity of mCP:PtON1:(CzBN or BCzBN) gradually decreased, possibly due to the concentration quenching of PtON1 itself. The PLQYs of mCP:1%(CzBN and BCzBN) films was as high as 99% and 95%, respectively. However, for mCP:30% PtON1:1%(CzBN and BCzBN) films, the PLQY decreased to 83% and 84% (see Tab. S1). Additionally, the PL spectra of PtON1 in mCP with different doping concentrations were tested. At the doping concentration of 5%, 20%, and 30%, the peak wavelengths were observed at 461, 464, 468 nm, respectively (see Fig. S1).

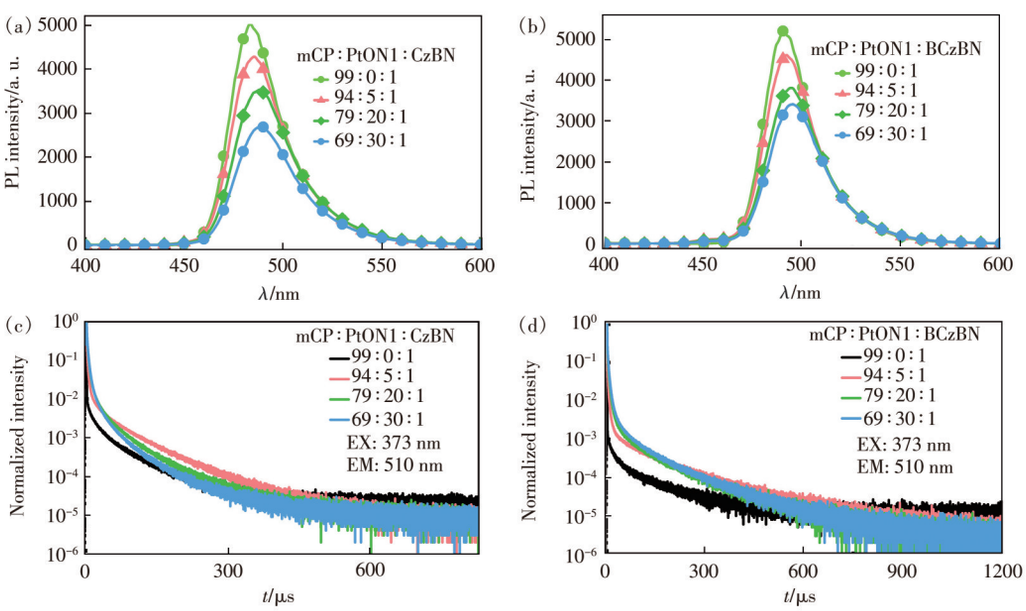

Fig.3 PL spectra of the emitting layers with different sensitizer concentrations, mixed with the guest emitters of CzBN(a) and BCzBN(b), respectively. Transient PL spectra of the sensitized films with CzBN(c) and BCzBN(d), respectively, detected at 510 nm under the excitation of 373 nm UV light

To investigate the excited states decay process in the films without and with the sensitizer, the transient PL decay curves were measured and shown in Fig. 3(c) and 3(d), respectively. As PtON1 doping concentration increased from 0% to 30%, the prompt lifetime gradually increased, and the delayed lifetime decreased, which clearly verified the proposed luminescent mechanisms shown in Fig. 1(b). The extended prompt decay lifetime indicated the exciton transfer from the triplet state of PtON1 to the singlet state of MR-TADF emitter. Concurrently, the shortened delayed lifetime was presumably due to the promoted triplet up-conversion of the MR-TADF emitter *via* RISC process, in the perturbation of the fast decay of PtON1.

Experimentally, for the PtON1 sensitized CzBN films, the delayed lifetime changed from 52.8 μs to 24.2 μs, and for the PtON1 sensitized BCzBN films, it dropped solidly from 98.3 μs to 57.4 μs. In the 30% PtON1 sensitized CzBN and BCzBN systems, the rates of FRET (k_{FRET}) were 1.1×10^6 s^{-1} and 3.2×10^6 s^{-1}, respectively, significantly surpassing the rates of k_{RISC} for the MR emitters. To demonstrate efficient FRET, we chose 450 nm as the detection wavelength to monitor the changes of the exciton lifetime of

PtON1. At this wavelength, there was almost no emission from CzBN and BCzBN, while PtON1 still displayed strong emission. As shown in Fig. S2, we examined the transient PL decays of mCP: 30% PtON1 and mCP: 30% PtON: 1% (CzBN and BCzBN), respectively. The averaged exciton lifetime of mCP: 30% PtON film was 1.6 μs, and those of the PtON1 sensitized CzBN and BCzBN films were shortened to 564.9 ns and 259.5 ns, respectively. This further confirmed the effective FRET process between the sensitizer and the emitters. It is because the emission of PtON1 was efficiently quenched at the presence of the MR-TADF. Additionally, the transient PL spectra of mCP: PtON1 in film at higher doping concentrations indicated the faster radiative decay of the triplet excitons(see Fig. S3).

To evaluate the electroluminescence(EL) of PtON1, the solution-processed OLEDs were fabricated based on the general configuration of indium tinoxide (ITO)/modified poly(3,4-ethylenedioxythiophene)-doped poly(styrene sulfonate) (PEDOT: PSS-HJ-1) (50 nm)/mCP: (5% for Device A1, 10% for Device A2, 20% for Device A3, and 30% for Device A4, respectively) PtON1/DPEPO (10 nm)/TmPyPB(50 nm)/Liq(1 nm)/Al (100 nm). The device structure was illustrated in Fig. 4(a). The EL data had been summarized in Tab. 2.

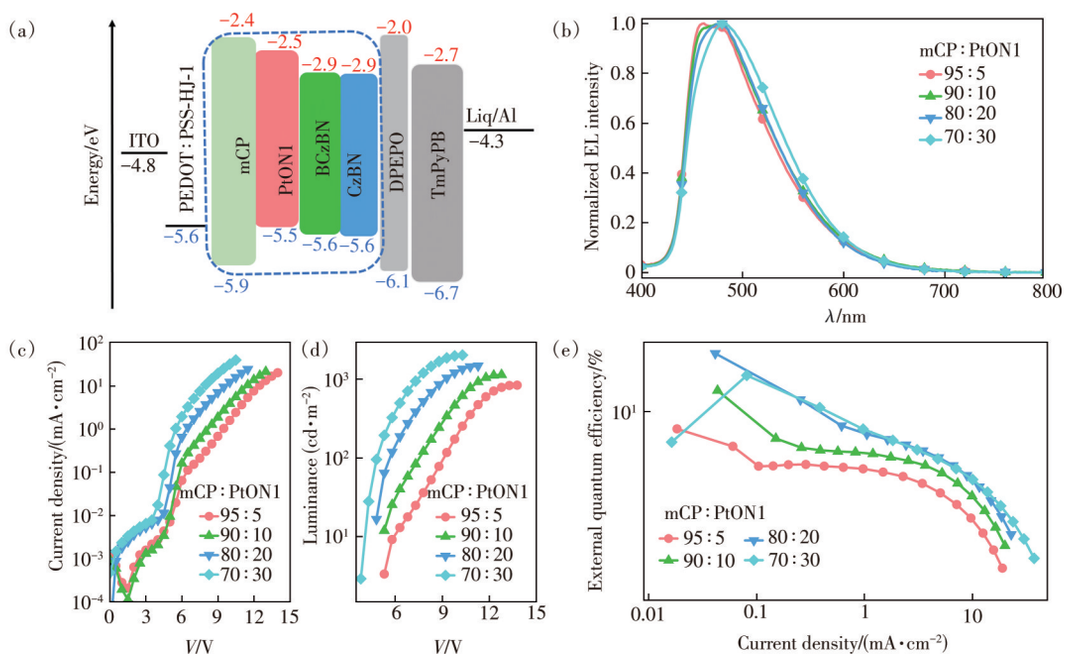

Fig.4 (a)Energy level alignment of the devices. EL performance of the devices A1−A4, respectively. Normalized EL spectra(b), current density-voltage(c), luminance-voltage curves(d), and external quantum efficiency-current density curves(e)

Tab. 2 Summary of the EL data of the devices A1−A4 with different doping concentrations of PtON1 in mCP

Device	V_{on}[a]/V	EQE_{max}[b]/%	CE_{max}[c]/(cd·A^{-1})	λ[d]/nm	CIE (x, y)[e]	FWHM[f]/nm
A1	5.5	8.4	16.8	476	(0.19, 0.28)	92
A2	5.5	12.3	25.3	477	(0.19, 0.30)	91
A3	5.0	17.9	37.3	478	(0.19, 0.31)	93
A4	4.0	14.3	14.3	480	(0.20, 0.34)	101

[a]Driving voltage at 1 cd/m^2. [b]Maximum EQE. [c]Maximum current efficiency. [d]EL peak wavelength. [e]The Commission International de I'Eclairage (CIE) 1931 color coordinates recorded at 8 V. [f]Full-width at half-maximum of EL spectrum.

At a low doping concentration of 5%, the device A1 with PtON1 as guest emitter displayed a EL peak at 462 nm with a broad FWHM of 91 nm. As the doping concentration of PtON1 increased, the EL spectrum was gradually red-shifted, following an increase in FWHM(see Fig. 4(b)). Fig. 4(c) and 4(d) presented the current density-voltage (J-V) and luminance-voltage (L-V) characteristics of the devices A1−

A4, respectively. The current density gradually increased with the increasing doping concentration of PtON1. As shown in Tab. 2, the turn-on voltage was 5.5 V for the device A1 with 5% PtON1 and then decreased to 4.0 V for the case with 30% PtON1 in mCP. The improvement was likely attributed to the high mobility of PtON1. At a concentration of 20%, *i.e.*, the device A2, the maximum EQE reached 17.9%. As indicated in Tab. 2 and Fig. 4(c), the overall EL performances have been remained at high doping concentration of PtON1, which would ease the device fabrication and reduce batch-to-batch deviation.

To exemplify the performance of PtON1 as the sensitizer, the solution-processed OLEDs with the blue MR-TADF emitter of CzBN were fabricated firstly while the organic materials (see Fig. 5(a)) above the emissive layer were consecutively evaporated to guarantee the excellent morphology and charge transport. The device structure was identical to the previous one mentioned above, except for the emissive layer, which was composed of mCP: (0% for Device B1, 5% for Device B2, 20% for Device B3, and 30% for Device B4, respectively) PtON1: 1% CzBN. The doping concentration of the MR-TADF emitter was fixed at 1% due to the serious concentration quenching effect.

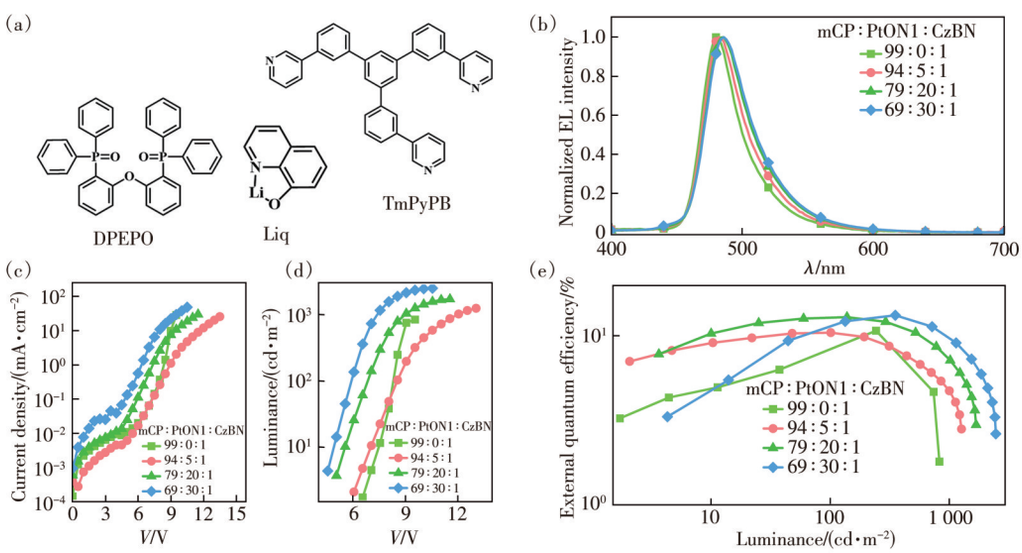

Fig.5 (a) Chemical structures of thermally evaporated organic materials used in this investigation. (b) Normalized EL spectra of the devices B1–B4 with mCP: PtON1 (0%, 5%, 20%, and 30%, respectively): CzBN as the emitting layers. Current density (c) and luminance (d) *vs.* driving voltage curves. (e) EQE *vs.* luminance curves of the devices

Fig. 5(b)–5(e) compared the EL spectra, *J-V-L* characteristics, and EQE-*J* curves of the devices B1–B4 with CzBN. The EL spectra were basically consistent with their PL spectra of films under photoexcitation, manifesting completely energy transfer from PtON1 to CzBN. Upon increasing the doping concentration of the sensitizer PtON1, the peak wavelength of the device with CzBN was shifted from 480 nm to 486 nm, followed with the enlarged FWHMs from 29 nm to 36 nm. This was due to aggregation and intermolecular interaction of the sensitizer. As the doping concentration of PtON1 increased, the current density increased. The device B4 with 30% PtON1: 1% CzBN in mCP achieved the lowest turn-on voltage of 4.5 V, attributed to excellent charge transport properties of PtON1. As shown in Fig. 5(e), the device B4 obtained the maximum EQE of 13.2% and the lowest efficiency roll-off of 25.8% at 1 000 cd/m^2, demonstrating superior performance, compared with those of the device B1 without the sensitizer. The alleviation of the efficiency roll-off of the device B4 was mainly attributed to the sensitization by PtON1, which reduced the exciton lifetime and accelerated the triplet harvesting. Thereby, the alleviated efficiency roll-off was achievable.

In phosphorescence-sensitized OLEDs, the distance between the PtON1 and the MR emitter significantly influenced the DET process. Therefore, DET can be inhibited by using BCzBN with the steric

hindrance effect, aiming to reduce energy loss. BCzBN and CzBN had the similar molecular skeleton. As shown in Fig. S4, the devices were constructed with 1% BCzBN as the MR-TADF emitter. As shown in Fig. S4(a), the EL spectrum of the device C1 without PtON1 is almost identical to that of the device C2. The EL spectra of the devices C3–C4 were slightly red-shifted. In Fig. S4(b) and S4(c), with the increasing concentration of PtON1, the tendency in current density and brightness for the devices C1–C4 were similar to those of the devices B1–B4, which were related to the enhanced charge transport at the presence of PtON1.

Moreover, owing to the steric hindrance of the peripheral groups in BCzBN, the distance between the sensitizer and MR-TADF emitter was increased, suppressing DET between PtON1 and the MR-TADF emitter. When PtON1 was fixed at 30%, the sensitized device realized the maximum EQE of 13.6%. However, the FWHM was slight enhanced to 36 nm due to the bathochromic shift of PtON1 as the high doing concentration. Compared with the device C1 with PtON1, the devices C2–C4 rendered the alleviated efficiency roll-offs at 1 000 cd/m^2 (see Tab. 3). The exciton utilization efficiency was estimated and compared in Tab. 3. For example, the exciton utilization efficiency of the devices B4 and C4 are 53.0% and 54.0%, respectively. This indicates that the low exciton utilization efficiency limits the device efficiency although the PLQY of the emissive layer is high. Most likely, it is attributed to the imbalance of charge carrier injection into the emissive zone.

Tab. 3　Summary of the EL data of the device series B1-B4 and C1–C4

Device	V_{on}[a]/V	EQE_{max}[b]/%	CE_{max}[c]/(cd·A^{-1})	λ[d]/nm	CIE (x, y)[e]	FWHM[f]/nm	Roll-off[g]/%	η_{eue}[h]/%
B1	6.5	10.7	17.5	480	(0.12, 0.29)	33	N.A.	36.0
B2	6.0	10.4	18.7	482	(0.12, 0.32)	36	53.8	36.9
B3	5.0	12.9	24.8	486	(0.13, 0.30)	39	43.4	50.6
B4	4.5	13.2	25.9	486	(0.13, 0.36)	40	25.8	53.0
C1	6.5	11.8	22.2	488	(0.11, 0.38)	33	N.A.	41.4
C2	6.0	10.2	19.8	488	(0.11, 0.39)	33	62.7	38.2
C3	5.0	11.7	24.3	492	(0.12, 0.40)	36	49.6	44.8
C4	4.5	13.6	28.9	492	(0.12, 0.43)	36	45.6	54.0

[a]Driving voltage at 1 cd/m^2. [b]Maximum value of external quantum efficiency (EQE). [c]Current efficiency (CE). [d]EL peak wavelength. [e]The Commission International de l'Eclairage (CIE)1931 color coordinates recorded at 10 V. [f]Full width at half-maxima of EL emission. [g]Efficiency roll-off at 1 000 cd/m^2. N.A.: not available. [h]Exciton utilization efficiency assuming the ideal charge balance and an out-coupling efficiency of 0.3.

4　Conclusion

In summary, we have demonstrated the efficient solution-processed blue narrowband OLEDs with the alleviated efficiency roll-offs by introducing the PtON1 phosphorescent sensitization with the short exciton lifetime. In addition, the intermolecular distance regulated by either the sensitizer doping concentration or steric hindrance effect of the guest molecule is useful to promote FRET. The detailed TRPL analysis reveals the phosphorescent sensitizer PtON1 efficiently facilitated the faster FRET process, converting triplet excitons to singlet excitons, in contrast to the slow RISC process on the MR emitter itself. This approach mitigates energy loss caused by exciton quenching, consequently enhancing exciton utilization efficiency. The solution-processed narrowband blue device exhibited the small FWHM less than 40 nm, high EQE of 13.2%, and small efficiency roll-off of 25.8% when PtON1 was used to sensitize CzBN. Moreover, inhibiting DET process from sensitizer to MR-TADF emitter BCzBN with the steric hindrance groups turns to be feasible. Consequently, the efficiency of the PtON1-sensitized BCzBN device was further improved to 13.6%. This provides a cost-effective route to regulate the electroluminescent performance of OLEDs.

Supplementary Information and Response Letter are available for this paper at: http://cjl.lightpublishing.cn/thesisDetails#10.37188/CJL.20240049.

References:

[1] YU Y, XING H, LIU D, *et al*. Solution-processed AIEgen NIR OLEDs with EQE approaching 15% [J]. *Angew. Chem. Ed. Int.*, 2022, 61(26): e202204279.

[2] SATOH C, OKADA T, OONO T, *et al*. Bandgap engineering for ultralow-voltage operation of organic light-emitting diodes [J]. *Adv. Opt. Mater.*, 2023, 11(20): 2300683.

[3] FAN X C, WANG K, SHI Y Z, *et al*. Thermally activated delayed fluorescence materials for nondoped organic light-emitting diodes with nearly 100% exciton harvest [J]. *SmartMat*, 2023, 4(1): e1122.

[4] WANG Z H, DONG S L, YUAN W Q, *et al*. Photo-modulated ionic polymer as an adaptable electron transport material for optically switchable pixel-free displays [J]. *Adv. Mater.*, 2024, 36(1): 2309593.

[5] YAO L Q, QIN Y, LI X C, *et al*. High-efficiency stretchable organic light-emitting diodes based on ultra-flexible printed embedded metal composite electrodes [J]. *InfoMat*, 2023, 5(5): e12410.

[6] JIANG R M, QIU N L, LI J S, *et al*. Efficient red delayed fluorescence molecule based on cyano-substituted 11,12-diphenyldibenzo[*a*, *c*] phenazine acceptor for high-performance organic light-emitting diodes [J]. *Innovation Mater.*, 2023, 1(1): 100012.

[7] BALDO M A, O'BRIEN D F, YOU Y, *et al*. Highly efficient phosphorescent emission from organic electroluminescent devices [J]. *Nature*, 1998, 395(6698): 151-154.

[8] ZHANG N, QU L, HU H, *et al*. Sky blue and yellow cluster light-emitting diodes based on asymmetric Cu_4I_4 nanocubes [J]. *Research*, 2022, 2022: 0005.

[9] NI H X, SUN W D, LUO X F, *et al*. Peripherally non-planar multiple resonance induced thermally activated delayed fluorescence materials containing silyl units [J]. *Innovation Mater.*, 2023, 1(3): 100041.

[10] UOYAMA H, GOUSHI K, SHIZU K, *et al*. Highly efficient organic light-emitting diodes from delayed fluorescence [J]. *Nature*, 2012, 492(7428): 234-238.

[11] YANG L, KIM V, LIAN Y X, *et al*. High-efficiency dual-dopant polymer light-emitting diodes with ultrafast inter-fluorophore energy transfer [J]. *Joule*, 2019, 3(10): 2381-2389.

[12] ZHAN L S, YING A, QI Y Y, *et al*. Copper(I) complex as sensitizer enables high-performance organic light-emitting diodes with very low efficiency roll-off [J]. *Adv. Funct. Mater.*, 2021, 31(48): 2106345.

[13] RYU C H, KIM S C, KIM M, *et al*. Novel tetradentate platinum(Ⅱ) complexes and their use in blue phosphorescent organic light-emitting diodes [J]. *Adv. Opt. Mater.*, 2022, 10(24): 2201799.

[14] CHEN L, TANG X, LIU R H, *et al*. Double-locked narrowband hybrid locally-excited and charge-transfer emitter exhibiting amplified spontaneous emission [J]. *Innovation Mater.*, 2023, 1(2): 100026.

[15] WU X, PENG X L, CHEN L T, *et al*. Through-space conjugated molecule with dual delayed fluorescence and room-temperature phosphorescence for high-performance OLEDs [J]. *ACS Mater. Lett.*, 2023, 5(3): 664-672.

[16] WU X, ZENG J J, PENG X L, *et al*. Robust sky-blue aggregation-induced delayed fluorescence materials for high-performance top-emitting OLEDs and single emissive layer white OLEDs [J]. *Chem. Eng. J.*, 2023, 451: 138919.

[17] ZHOU L, NI F, LI N, *et al*. Tetracoordinate boron-based multifunctional chiral thermally activated delayed fluorescence emitters [J]. *Angew. Chem.*, 2022, 134(28): e202203844.

[18] KONDO Y, YOSHIURA K, KITERA S, *et al*. Narrowband deep-blue organic light-emitting diode featuring an organoboron-based emitter [J]. *Nat. Photonics*, 2019, 13(10): 678-682.

[19] TANG Y, XIE G H, LIANG X, *et al*. Organic and quantum-dot hybrid white LEDs using a narrow bandwidth blue TADF emitter [J]. *J. Mater. Chem. C*, 2020, 8(31): 10831-10836.

[20] TAN H J, YANG G X, DENG Y L, *et al*. Deep-blue OLEDs with Rec. 2020 blue gamut compliance and EQE over 22% achieved by conformation engineering [J]. *Adv. Mater.*, 2022, 34(18): 2200537.

[21] WANG T, YIN X J, CAO X S, *et al*. A simple approach to solution-processible small-molecule multi-resonance TADF emitters for high-performance narrowband OLEDs [J]. *Angew. Chem. Int. Ed.*, 2023, 62(24): e202301988.

[22] YE Z Y, WU H, XU Y L, *et al*. Deep-blue narrowband hetero[6]helicenes showing circularly polarized thermally activated delayed fluorescence toward high-performance OLEDs [J]. *Adv. Mater.*, 2024, 36(1): 2308314.

[23] CHEN L, CHANG Y F, SHU H Y, *et al*. Achieving efficient solution-processed blue narrowband emitting OLEDs with small efficiency roll-off by using a bulky TADF sensitizer with high reverse intersystem crossing rate [J]. *Adv. Opt. Mater.*, 2023,

11(2): 2201898.

[24] KIM H G, KIM K H, KIM J J. Highly efficient, conventional, fluorescent organic light-emitting diodes with extended lifetime [J]. *Adv. Mater.*, 2017, 29(39): 1702159.

[25] 高羽晗, 谢国华. 级联敏化三元旋涂型磷光器件电致发光性能 [J]. 发光学报, 2023, 44(2): 219-226.
GAO Y H, XIE G H. Electroluminescent performances of solution-processed phosphorescent organic light-emitting diodes based on cascade energy transfer of ternary blends [J]. *Chin. J. Lumin.*, 2023, 44(2): 219-226. (in Chinese)

[26] LEE K H, LEE J Y. Phosphor sensitized thermally activated delayed fluorescence organic light-emitting diodes with ideal deep blue device performances [J]. *J. Mater. Chem.* C, 2019, 7(28): 8562-8568.

[27] LIN C W, HAN P B, XIAO S, *et al.* Efficiency breakthrough of fluorescence OLEDs by the strategic management of "Hot Excitons" at highly lying excitation triplet energy levels [J]. *Adv. Funct. Mater.*, 2021, 31(48): 2106912.

[28] SONG X Z, ZHANG D D, LU Y, *et al.* Understanding and manipulating the interplay of wide-energy-gap host and TADF sensitizer in high-performance fluorescence OLEDs [J]. *Adv. Mater.*, 2019, 31(35): 1901923.

[29] WU Z L, SONG S X, ZHU X Y, *et al.* Highly efficient deep-blue fluorescent OLEDs based on anthracene derivatives with a triplet-triplet annihilation mechanism [J]. *Mater. Chem. Front.*, 2021, 5(18): 6978-6986.

[30] XIAO S, QIAO X F, LIN C W, *et al.* In situ quantifying the physical parameters determining the efficiency of OLEDs relying on triplet-triplet annihilation up-conversion [J]. *Adv. Opt. Mater.*, 2022, 10(6): 2102333.

[31] YIU T C, GNANASEKARAN P, CHEN W L, *et al.* Multifaceted sulfone-carbazole-based D-A-D materials: a blue fluorescent emitter as a host for phosphorescent OLEDs and triplet-triplet annihilation up-conversion electroluminescence [J]. *ACS Appl. Mater. Interfaces*, 2023, 15(1): 1748-1761.

[32] BRAVEENTH R, LEE H, PARK J D, *et al.* Achieving narrow FWHM and high EQE over 38% in blue OLEDs using rigid heteroatom-based deep blue TADF sensitized host [J]. *Adv. Funct. Mater.*, 2021, 31(47): 2105805.

[33] LI D L, YANG J J, CHEN J T, *et al.* Efficient narrowband green OLEDs with TADF sensitizers combining multiple charge-transfer pathways [J]. *Mater. Chem. Front.*, 2023, 7(6): 1128-1136.

[34] TANG R, XU S, DU L L, *et al.* Au(Ⅰ)-TADF emitters for high efficiency full-color vacuum-deposited OLEDs and TADF-sensitized fluorescent OLEDs with ultrahigh brightness and prolonged operational lifetime [J]. *Adv. Opt. Mater.*, 2023, 11(23): 2300950.

[35] LIU T X, XIE G H, ZHONG C, *et al.* Boosting the efficiency of near-infrared fluorescent OLEDs with an electroluminescent peak of nearly 800 nm by sensitizer-based cascade energy transfer [J]. *Adv. Funct. Mater.*, 2018, 28(18): 1706088.

[36] HEIMEL P, MONDAL A, MAY F, *et al.* Unicolored phosphor-sensitized fluorescence for efficient and stable blue OLEDs [J]. *Nat. Commun.*, 2018, 9(1): 4990.

[37] KIM S C, RYU C H, LEE K M, *et al.* Tetradentate Pt(Ⅱ) complex as phosphorescent sensitizer for highly efficient green organic light-emitting diodes with low efficiency roll-off [J]. *Adv. Opt. Mater.*, 2023, 11(13): 2202698.

[38] KIM H G, SHIN H, HA Y H, *et al.* Triplet harvesting by a fluorescent emitter using a phosphorescent sensitizer for blue organic-light-emitting diodes [J]. *ACS Appl. Mater. Interfaces*, 2019, 11(1): 26-30.

[39] NAM S, KIM J W, BAE H J, *et al.* Improved efficiency and lifetime of deep-blue hyperfluorescent organic light-emitting diode using Pt(Ⅱ) complex as phosphorescent sensitizer [J]. *Adv. Sci.*, 2021, 8(16): 2100586.

[40] TAO Y, YUAN K, CHEN T, *et al.* Thermally activated delayed fluorescence materials towards the breakthrough of organoelectronics [J]. *Adv. Mater.*, 2014, 26(47): 7931-7958.

[41] LEE S, KIM H, KIM Y. Progress in organic semiconducting materials with high thermal stability for organic light-emitting devices [J]. *InfoMat*, 2021, 3(1): 61-81.

[42] WANG Y X, GUO R D, YING A, *et al.* Multiple-resonance-type TADF emitter as sensitizer improving the performance of blue fluorescent organic light-emitting diodes [J]. *Adv. Opt. Mater.*, 2023, 11(1): 2202034.

[43] WANG Y X, DUAN Y L, GUO R D, *et al.* A periphery cladding strategy to improve the performance of narrowband emitters, achieving deep-blue OLEDs with CIE_y< 0.08 and external quantum efficiency approaching 20% [J]. *Org. Electron.*, 2021, 97: 106275.

[44] HANG X C, FLEETHAM T, TURNER E, *et al.* Highly efficient blue-emitting cyclometalated platinum(Ⅱ) complexes by judicious molecular design [J]. *Angew. Chem. Int. Ed.*, 2013, 52(26): 6753-6756.

[45] XU S, YANG Q Q, ZHANG Y, *et al*. Solution-processed multi-resonance organic light-emitting diodes with high efficiency and narrowband emission [J]. *Chin. Chem. Lett.*, 2021, 32(4): 1372-1376.

李家乐(2000-),男,安徽阜阳人,硕士研究生,2021年于延边大学获得学士学位,主要从事有机光电材料和器件方面的研究。

E-mail: jialeli@whu.edu.cn

谢国华(1982-),男,福建漳州人,博士,教授,博士生导师,2011年于吉林大学获得博士学位,主要从事有机光电材料与器件的研究。

E-mail: ifeghxie@xmu.edu.cn

龚少龙(1984-),男,湖北汉川人,博士,教授,博士生导师,2012年于武汉大学获得博士学位,主要从事新型(金属)有机发光材料的设计合成、结构与性能及其光电应用的研究。

E-mail: slgong@whu.edu.cn